

Ultra-Wideband Silicon Photonic BiCMOS Coherent Receiver for O- and C-Band

Pascal M. Seiler^(1,2), Karsten Voigt^(2,1), Stefan Lischke⁽²⁾, Andrea Malignaggi⁽²⁾ and Lars Zimmermann^(1,2)

⁽¹⁾ Technische Universität Berlin, Chair of Siliziumphotonik, Straße des 17. Juni 135, 10623 Berlin, Germany, seiler@tu-berlin.de

⁽²⁾ IHP - Leibniz-Institut für innovative Mikroelektronik, Im Technologiepark 25, 15236 Frankfurt (Oder), Germany

Abstract In this work, we present a dual window silicon photonic coherent receiver for O- and C-band, fabricated in a 0.25 μm BiCMOS technology. Performance is evaluated for up to 50 Gb/s, while utilizing a local oscillator power of up to 6.9 dBm.

Introduction

Traditionally, there was a clear distinction between direct-detect data center interconnects (DCIs, O-band) and long-haul coherent communication (C-band). However, the potential deployment of coherent links in the data center domain has gained significant interest in recent years. The border between coherent and direct-detect systems is subject of intense debate. Shorter coherent links may even benefit from O-band coherent photonics^[1], further blurring the divide between O- and C-band communication. Recently, broadband optical conversion from C- to O-band by nonlinear four-wave mixing in multi-mode silicon waveguides^[2], and very high-speed hybrid lithium niobate/silicon modulator for C- to O-band^[3] were demonstrated, rendering the entire wavelength range between O- and C-band transparent to coherent formats. Considering the convergence of coherent communication across optical bands spanning more than 200 nm, cost-efficient ultra-wideband high-speed coherent receivers may become a necessity.

In this work, we will present the first monolithic silicon photonic BiCMOS dual window coherent receiver, fabricated in IHP's 0.25 μm photonic BiCMOS technology. In contrast to the work in Ref. [4], the demonstrated receiver in this work monolithically co-integrates an electronic amplifier stage and is characterized at up to 50 Gb/s. The receiver features a 2×2 MMI network as 90° hybrid with a central wavelength of 1430 nm. In principle, the receiver can be used in the E- and S-band as well, since these are closer to the MMI network's central wavelength.

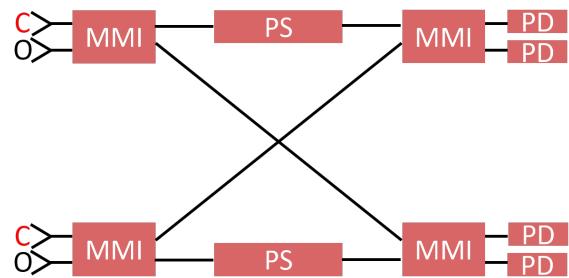


Fig. 1: 2×2 MMI coupler network used for the coherent receiver. MMI: multi-mode interference coupler, PS: phase shifter, PD: photodiode.

O/C-Band Coherent Receiver

A schematic of the optical circuit is shown in Fig. 1. Optical coupling is achieved by focusing 1-dimensional grating coupler. The choice of grating coupler for this prototype was done given their reliability, and the possibility of on-wafer testing. However, in a future iteration, broadband optical interfaces suitable for O- and C-band, i.e. spot-size converter, should be implemented. The additional integration of polarization-rotator splitter would also enable dual polarization applications. While in dedicated O- or C-band coherent receivers, 4×4 MMI coupler may be used as 90° hybrid^[5], the imbalance and phase error quickly rise to impractical levels when deviating too far from the design wavelength. Therefore, the hybrid is realized using a 2×2 MMI network^{[6],[7]}, which offers a larger optical bandwidth in comparison to 4×4 MMIs^[8]. However, an additional phase shift of 90° is required for a proper separation of in-phase and quadrature component. Here, this phase shift is controlled using metal heaters placed above the silicon waveguides. The simulated performance for one of the 2×2 MMIs is given in Fig. 2. From O- to C-band, the imbalance between the two output ports is at worst

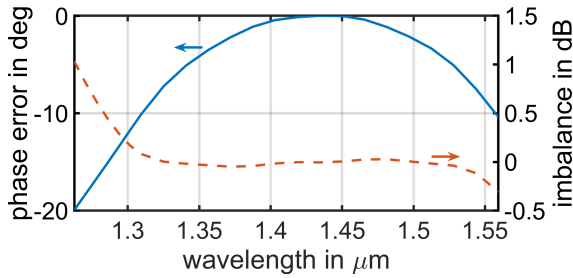


Fig. 2: Simulated MMI performance. The phase error is expressed as the difference in phase at one output when using either input port 1 or 2 relative to the ideal phase difference of 90° .

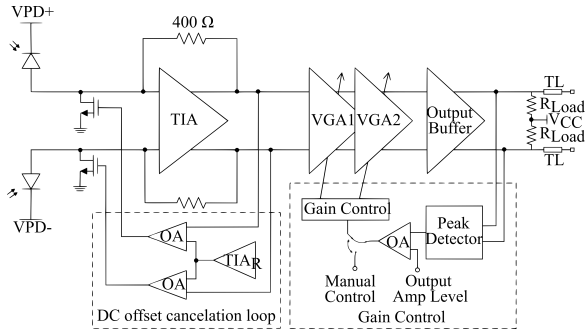


Fig. 3: Electrical section of the coherent receiver. The circuit is shown only for one channel, whereas an identical circuit is used for the second channel. OA: operational amplifier, TIA: transimpedance amplifier, TIA_R : Replica TIA, VGA: variable gain amplifier, TL: transmission line, VPD: photodiode bias voltage.

1 dB. The phase error is expressed as the difference in phase at one output when using either input port 1 or 2 relative to the ideal phase difference of 90° . At 1310 nm and 1550 nm, the error is approximately 10° . The optical network is terminated by single-ended photodiodes. The electrical circuit (per channel) is shown in Fig. 3. It consists of an input stage, two variable gain amplifiers (VGAs) and a $50\ \Omega$ output buffer. It features a DC cancellation loop and a manual- and automatic gain control. Further information on the circuit topology may be found in Ref. [9]. The total power consumption for the electrical circuit is approximately 449 mW. The additional power consumption for the metal heater required for the 90° phase shift is typically below 10 mW. The chip area of the coherent receiver is approximately $6\ \text{mm}^2$. The opto-electrical bandwidth was determined on a dedicated O-band coherent receiver with an identical electrical circuit on the same wafer. A measured normalized response is shown in Fig. 4, indicating a 3 dB bandwidth of approximately 30 GHz. The bandwidth was measured using the beating of two external-cavity laser (ECL) and a RF power meter. The system performance of the receiver is verified in an intradyne back-to-back experiment, with the setup shown in Fig. 5. A dedicated

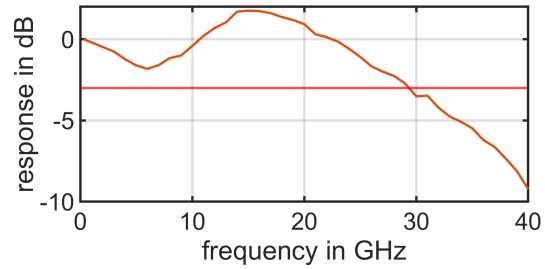


Fig. 4: Opto-electrical bandwidth of a dedicated O-band coherent receiver with an identical electrical circuit on the same wafer.

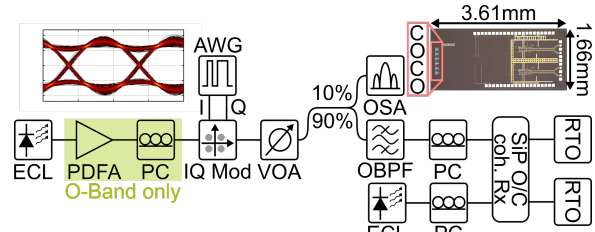


Fig. 5: Intradyne measurement setup with integrated O/C-band coherent receiver. A QPSK signal is applied using a commercial C-band IQ-modulator (IQ Mod). The top left inset shows the electrical eye diagram supplied by the AWG at 50 Gb/s, and a chip photograph is shown in the top right. PC: polarization controller, OSA: optical spectrum analyzer, PDFFA: praseodymium-doped fiber amplifier, OBPF: optical bandpass filter (1 nm).

C-band IQ-modulator with an integrated C-band laser (ID Photonics OMFT, 1545 nm) is supplied with a $400\ \text{mV}_{PP}$ quadrature-phase shift-keying (QPSK) signal from an arbitrary waveform generator (AWG, Keysight M8199A, 256 GSa/s). An electrical eye diagram at 50 Gb/s is shown as inset in the top left in Fig. 5. The optical signal is then attenuated using a variable optical attenuator (VOA, Keysight N7752A) to vary the received optical power (ROP) during the experiment. Single-ended electrical signals from the receiver are connected to two real-time oscilloscopes (Tektronix DPO77002SX, 200 GSa/s, 40 GHz 3 dB bandwidth). During the O-band measurement, a separate ECL (1310 nm) is pre-amplified to partially compensate for the laser's lower output power and the higher losses of the C-band IQ modulator. Tektronix optical modulation analyzer software (OM1106D) is used for offline digital signal processing (DSP) and bit error rate (BER) measurements. The local oscillator (LO) power for the O- and C-band measurement is 6.5 dBm and 6.9 dBm, respectively. Determined BERs for varied ROPs are given in Fig. 6. For the O-band, symbol rates of 32 Gb/s, 40 Gb/s, and 50 Gb/s are measured. The performance of the receiver in the C-band is also verified by a 50 Gb/s QPSK measurement. Exemplary eye- and constellation diagrams are also shown in Fig. 7.

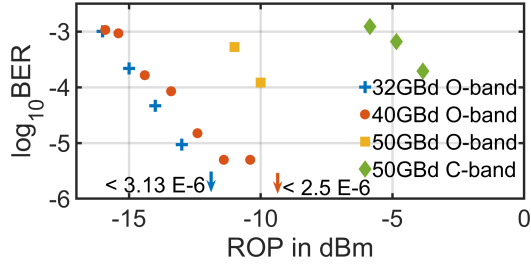


Fig. 6: BER versus ROP for different symbol rates in the O-band. Performance in the C-band is verified by a measurement at 50 GBd. The LO power for the O- and C-band measurement is 6.5 dBm and 6.9 dBm, respectively.

Discussion

The BERs in Fig. 6 show a similar performance for 32 GBd and 40 GBd in the O-band, with a penalty of around 1 dB. An increased penalty of approximately 3.5 dB can be found between the 40 GBd and 50 GBd transmission. Note, that a comparatively low LO power of +6.5 dBm is used in this experiment, which is advantageous in an intra DCI environment, where power consumption is a prime resource. Nonetheless, further improvements can be expected by a higher LO power, as well as a dedicated O-band IQ modulator. Due to the C-band IQ-modulator, a 6 dB stronger signal is available in the C-band at 50 GBd. While the performance is very similar to the O-band experiment despite that, it needs to be noted that the photo current for the C-band is also only about a quarter of the current in the O-band. This deviation can be attributed to two key factors. The fiber array used in this experiment is aligned to favor the O-band, since the data link at 1310 nm already suffers from a degradation due to the C-band IQ-modulator. Additionally, process variations can affect O- and C-band performance as well, e.g. due to differences in the photodiode responsivity. Presently, this difference could be compensated using a stronger local oscillator. Given the deployment of C-band coherent links in the long-haul domain, the additional power consumption for this increase is even more feasible than in the O-band. An unresolved issue are contact instabilities due to the large number of pads which need to be probed during the experiment, which shall be improved in the future by a packaged solution. Despite these temporary issues, the receiver demonstrates promising performance in the O- and C-band, thus potentially enabling coherent communication over more than 200 nm bandwidth.

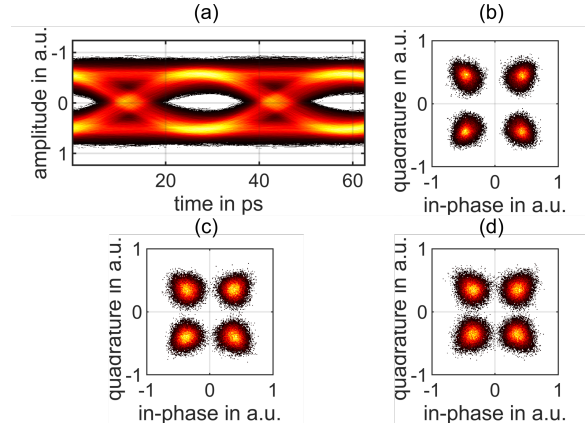


Fig. 7: (a) Recovered eye diagram and (b) constellation at 32 GBd in the O-band (ROP = -9 dBm). The eye diagram has been interpolated. 50 GBd constellation in the (c) O-band (ROP = -10 dBm) and (d) C-band (ROP = -3.9 dBm).

Conclusions

The O- and C-band coherent receiver demonstrated in this work has been characterized at up to 50 GBd. At 40 GBd, the receiver shows 6.5 dB power budget for a ROP of -9 dBm. This translates to the loss of approximately 20 km standard single mode fiber at 1310 nm. The deviation towards higher symbol rates in the C-band can be attributed to setup- and process variations, e.g. the coupling efficiency and photodiode responsivity. We therefore expect to approach state of the art performance of dedicated C-band coherent receiver for a higher LO power and improved packaging solution, i.e. contacting and optical interface. While respective optical sources were presently unavailable, the receiver could in principal be used in the E- and S-band as well, since these are closer to the MMI network's central wavelength of 1430 nm.

Acknowledgements

This work was supported in part by the German Research Foundation (DFG) through the projects EPIC-Sense (ZI 331 1283-6-1) and EPIDAC (ZI 1283-7-1), by the Federal Ministry of Education and Research (BMBF) through project 332 PEARLS (13N14936), and the European Commission through project H2020-SPACE-ORIONAS (822002).

References

- [1] P. M. Seiler, G. Georgieva, G. Winzer, A. Peczek, K. Voigt, S. Lischke, A. Fatemi, and L. Zimmermann, "Towards Coherent O-Band Data Center Interconnects", *Frontiers of Optoelectronics*, to be published.
- [2] G. Ronniger, I. Sackey, T. Kernetzky, U. Höfler, C. Mai, C. Schubert, N. Hanik, L. Zimmermann, R. Freund, and K. Petermann, "Efficient Ultra-Broadband C-to-O Band Converter Based on Multi-Mode Silicon-on-

Insulator Waveguides”, in *2021 Eur. Conf. Opt. Commun. (ECOC), We1G.1, Bordeaux, France, 2021*.

- [3] S. Sun, M. He, M. Xu, S. Gao, S. Yu, and X. Cai, “Hybrid silicon and lithium niobate modulator”, *IEEE Journal of Selected Topics in Quantum Electronics*, vol. 27, no. 3, pp. 1–12, May 2021.
- [4] C. Doerr, L. Chen, T. Nielsen, R. Aroca, L. Chen, M. Banaee, S. Azemati, G. McBrien, S. Y. Park, J. Geyer, B. Guan, B. Mikkelsen, C. Rasmussen, M. Givehchi, Z. Wang, B. Potsaid, H. C. Lee, E. Swanson, and J. G. Fujimoto, “O, E, S, C, and L band silicon photonics coherent modulator/receiver”, in *Opt. Fiber Commun. Conf. Exhib. (OFC)*, OSA, 2016.
- [5] P. M. Seiler, A. Peczek, G. Winzer, K. Voigt, S. Lischke, A. Fatemi, and L. Zimmermann, “56 GBaud O-Band Transmission using a Photonic BiCMOS Coherent Receiver”, in *2020 Eur. Conf. Opt. Commun. (ECOC)*, 2020, pp. 1–4.
- [6] R. Kunkel, H.-G. Bach, D. Hoffmann, C. Weinert, I. Molina-Fernandez, and R. Halir, “First monolithic InP-based 90°-hybrid OEIC comprising balanced detectors for 100GE coherent frontends”, in *2009 IEEE Intl. Conf. Indium Phosphide Relat. Mater.*, IEEE, May 2009.
- [7] Y. Sakamaki, Y. Nasu, T. Hashimoto, K. Hattori, T. Saida, and H. Takahashi, “Reduction of phase-difference deviation in 90° optical hybrid over wide wavelength range”, *IEICE Electronics Express*, vol. 7, no. 3, pp. 216–221, 2010.
- [8] K. Voigt, L. Zimmermann, G. Winzer, and K. Petermann, “SOI based 2 × 2 and 4 × 4 waveguide couplers - evolution from DPSK to DQPSK”, in *2008 5th IEEE International Conference on Group IV Photonics*, IEEE, 2008.
- [9] A. Awny, R. Nagulapalli, M. Kroh, J. Hoffmann, P. Runge, D. Micusik, G. Fischer, A. C. Ulusoy, M. Ko, and D. Kissinger, “A linear differential transimpedance amplifier for 100-Gb/s integrated coherent optical fiber receivers”, *IEEE Trans. Microw. Theory Tech.*, vol. 66, no. 2, pp. 973–986, Feb. 2018.